Geoscience Frontiers 7 (2016) 419–430

HOSTED BY

ELSEVIER

Contents lists available at ScienceDirect

China University of Geosciences (Beijing)

Geoscience Frontiers

journal homepage: www.elsevier.com/locate/gsf

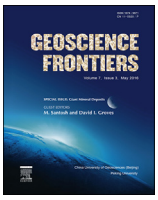

Research paper

World-class Xincheng gold deposit: An example from the giant Jiaodong gold province

Liqiang Yang [a,*], Jun Deng [a,*], Ruipeng Guo [b], Lin'nan Guo [a], Zhongliang Wang [a], Binghan Chen [a], Xudong Wang [c]

[a] State Key Laboratory of Geological Processes and Mineral Resources, China University of Geosciences, Beijing 100083, China
[b] Shandong Institute of Geological Survey, Jinan 250013, China
[c] Xincheng Gold Company, Shandong Gold Mining Stock Co., Ltd., Laizhou City 261438, Shandong Province, China

ARTICLE INFO

Article history:
Received 2 June 2015
Received in revised form
19 August 2015
Accepted 29 August 2015
Available online 8 October 2015

Keywords:
Xincheng gold deposit
Jiaodong Peninsula
China
Giant gold system
Gold genesis
Epizonal orogenic gold

ABSTRACT

The Jiaodong gold deposits are currently the most important gold resources (with Au reserves of >4000 t) in China, and the leading gold-producing country globally (with Au production of ~428 t in 2013). Jiaodong is also considered as perhaps the only world-class to giant gold accumulation on the planet where relatively young gold ores (ca. 130–120 Ma) were deposited in rocks that are 2 Ga older. The Xincheng world-class high-grade gold deposit, with a proven reserve of >200 t gold, is one of the largest deposits in the giant gold province of the Jiaodong Peninsula. It is located in the northwestern part of the Jiaobei Uplift, and hosted by ca. 132–123 Ma Xincheng quartz monzonites and monzogranites. Ore zones are structurally controlled by the NE-trending and NW-dipping Jiaojia Fault and subsidiary faults, and are mainly restricted to the footwall of the fault. The dominant disseminated- and stockwork-style ores are associated with strong sericitization, silicification, sulfidation and K-feldspathization, and minor carbonate wallrock alteration halos. The four mineralization stages are pyrite–quartz–sericite (stage 1), quartz–pyrite (stage 2), quartz–polysulfide (stage 3) and quartz–carbonate (stage 4). Gold occurs dominantly as electrum, with lesser amounts of sulfide-hosted native gold and rare native silver and argentite, normally associated with pyrite, chalcopyrite, galena and sphalerite: the latter with proven resources of about 105 t Ag, 713 t Cu, and 5100 t S.

There are three types of ore-related fluid inclusions: type 1 aqueous-carbonate (H_2O–CO_2), type 2 aqueous (liquid H_2O + vapor H_2O), and type 3 CO_2 (liquid CO_2 and vapor CO_2) inclusions. Homogenization temperatures range from 221 to 304 °C for type 1 inclusions, with salinities of 2.4–13.3 wt.% NaCl eq., and bulk densities of 0.858–1.022 g/cm^3. The $\delta^{34}S_{CDT}$ values of hydrothermal sulfides are 4.3–10.6‰ and $\delta^{18}O$ values of hydrothermal quartz have a median value of 13.0‰. δD values of fluid inclusions in hydrothermal quartz have a median value of −75‰. Calculated $\delta^{18}O_{water}$ has a median value of 5.2‰. The timing of gold mineralization at the Xincheng gold deposit is younger than 123 ± 1 Ma, and likely between 120.9 and 119.9 Ma.

A minerals system genetic model for the probable epizonal orogenic Xincheng deposit suggests an initial medium temperature, CO_2-rich, and low salinity H_2O–CO_2 deeply sourced metamorphic ore fluid associated with dehydration and decarbonization of subducting Paleo-Pacific lithosphere. The Jiaojia Fault constrained the migration of ore-forming fluids and metals at the brittle–ductile transition. Fluid immiscibility, caused by episodic pressure drops, led to significant high-grade gold deposition in the giant Xincheng gold deposit.

1. Introduction

The Jiaodong gold deposits are currently the most important gold resources (with Au reserves of >4000 t) in China (Yang et al., 2014a), the leading gold-producing country globally (with Au

* Corresponding authors. State Key Laboratory of Geological Processes and Mineral Resources, China University of Geosciences, No. 29 Xue-Yuan Road, Haidian District, Beijing 100083, China. Tel.: +86 10 8232 2301 (O); fax: +86 10 8232 1006.
E-mail addresses: lqyang@cugb.edu.cn (L. Yang), djun@cugb.edu.cn (J. Deng).
Peer-review under responsibility of China University of Geosciences (Beijing).

http://dx.doi.org/10.1016/j.gsf.2015.08.006

production of ~428 t in 2013, data from the China Gold Association website). Jiaodong is also considered as perhaps the only world-class to giant gold accumulation on the planet where relatively young gold ores (ca. 130–120 Ma; Goldfarb et al., 2014; Yang et al., 2016a) were deposited in rocks that are billions of years older (ca. 2.9–1.9 Ga; Jahn et al., 2008; Deng et al., 2011), during an anomalous lithospheric delamination event in which the Archean–Paleoproterozoic metamorphic basement of the North China Block was intruded by multiple pulses of Mesozoic granitic magmas (Yang et al., 2016b). The Xincheng gold deposit is situated in the northwestern part of the giant Jiaodong gold province, comprising currently the most important gold resources (>4000 t Au) in China (Yang et al., 2014a). Xincheng was discovered as a small gold deposit by drilling in 1971 by the No. 6 Geological Team of Shandong Bureau of Geology and Mineral Resources, China. This reconnaissance survey, combined with detailed investigation and exploration of the No. I orebody, was carried out from 1974 to 1987, and the mine was put into operation in 1979. Detailed investigation and exploration of the No. II orebody took place from 1988 to 1994. The Xincheng gold deposit is currently the largest gold deposit in Jiaodong, with a gold reserve of >200 t Au at a grade of 7.75 g/t Au, and is hosted within the early Cretaceous granitoids (L. Wang et al., 2014; Wang et al., 2014a, 2015; Yang et al., 2014b). A scientific study of this gold deposit was designed to help define the mechanism of formation of the Jiaodong gold deposits in general, and also help target additional large tonnage gold ores in the extensive late Mesozoic granitoids of the Jiaodong area (Goldfarb et al., 2014). This paper summarizes the available geological and geochemical data, including those recently obtained by us, and thereby clarifies the nature and mechanism of formation of the Xincheng gold deposit within a minerals system model.

2. Tectonic and metallogenic setting

2.1. Tectonic setting

The Jiaodong gold province is situated at the southeastern part of the North China Craton (NCC). The NCC is different from most cratons, which are characterized by a thick lithospheric root (>200 km) and low crustal heat flow, and lack internal magmatism and tectonism since their formation in the Precambrian (Artemieva and Mooney, 2001). In contrast, the NCC has been affected by multiple orogenesis in the Phanerozoic, and is characterized by multiple tectono-magmatic and metallogenic events during the Mesozoic (Deng et al., 2006; Yang et al., 2015a,b).

The crustal growth and stabilization of the NCC occurred during the Neoarchean, and the basement is dominated by tonalite–trondhjemite–granodiorite (TTG) gneiss, amphibolite, ultramafic bodies, and banded iron formations (Zhao et al., 2001). Subsequent Paleoproterozoic rifting, probably at 2.3–2.0 Ga, is recorded by a series of bimodal volcanic and sedimentary rocks (Zhai and Santosh, 2011; Tang et al., 2013). The NCC was finally stabilized at ca 1.85 Ga, during collision between the Western and Eastern Blocks, which are separated by the Trans-North China Orogen (Fig. 1; Zhao et al., 2001, 2005). Multistage rifting events occurred after the cratonization of the NCC, during the late Paleoproterozoic to Neoproterozoic. From the Paleozoic to early Mesozoic, the southern and northern margins of the NCC have been affected by multiple orogenesis (Chen et al., 2009; Dong et al., 2011). Thrusting and crustal thickening, caused by the closure of the Paleo-Asian Ocean, and continued convergence occurred on the northern margin of the NCC during the late Permian to early Jurassic (Xiao et al., 2003). Similarly, crustal thickening and continental subduction, caused by ocean closure and collision between the Yangtze Craton and the NCC, occurred in the Triassic to Jurassic, forming the Qinling–Dabie–Sulu Orogen (Dong et al., 2011), with 500–700 km sinistral slip across the Tan-Lu Fault (Fig. 1; Zhu et al., 2010). While the Western Block has been relatively stable, the Eastern Block has experienced extensional tectonic movements associated with lithospheric thinning and de-cratonization during the late Jurassic to early Cretaceous (Zhu et al., 2010), accompanied by large-scale magmatic activity and gold mineralization (Deng et al., 2014a, 2015).

2.2. Gold provinces of the North China Craton

Hundreds of lode gold deposits are distributed along the eastern, southern, and northern margins of the NCC, including the

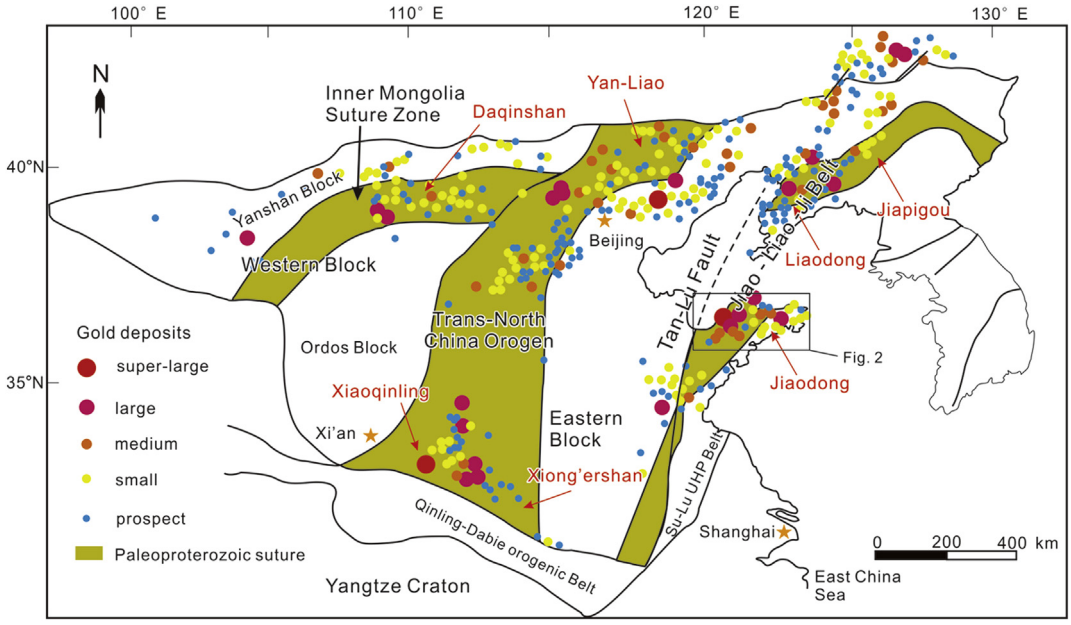

Figure 1. Tectonic framework of the North China Craton (modified from Li et al., 2012; Groves and Santosh, 2015), showing the distribution of gold deposits.

Jiao–Liao–Ji Belt, Xiaoqinling–Xiong'ershan and the Northern NCC gold district (Fig. 1), which provide China's major source of gold production (Li and Santosh, 2014; Groves and Santosh, 2015).

The Jiao–Liao–Ji Belt, comprising the Jiaodong gold province, Liaodong gold district and Jiapigou gold belt, is located on the eastern margin of the NCC and distributed along the Tan–Lu Fault (Fig. 1). The Jiaodong Peninsula, located in the southeast NCC, is the most important gold province of China, with more than 150 gold deposits within it having total proven gold resources of 4000 tons (Fig. 2; Yang et al., 2014a). These gold deposits are structurally controlled by regional NE–NNE detachment faults and are hosted by Mesozoic granitoids, with gold formation at about 130–110 Ma (Li et al., 2003; Yang et al., 2014c). Hydrothermal alteration is well developed and mainly characterized by sulfidation, sericitization, silicification, K-feldspar alteration and carbonation. Gold occurs in disseminated- and stockwork-style and auriferous quartz vein-style ores (Deng et al., 2003a; Goldfarb and Santosh, 2014; Yang et al., 2014a).

There are abundant gold deposits in the Liaodong Rift which formed by extension and fracturing of the crust in the Paleoproterozoic. These gold deposits are structurally controlled by contemporaneous faults and anticlinal folds, and are hosted in greenschist-facies interlayered carbonates rocks and fine-clastic rocks. They formed in the metallogenetic epoch from the Indosinian to Yanshanian. Ores are characterized by massive, disseminated, net-veined, brecciated and banded mineralization (Liu and Ai, 2000; Yang, 2000; Lin et al., 2013).

The Jiapigou gold belt is located in the Jiapigou shear zone in the northeastern wedge of the NCC, adjacent to a branch of the deep-seated Tan–Lu Fault. Gold mineralization is controlled by dextral-reverse strike-slip faults in an arcuate fault belt. The basement of the belt is Precambrian TTG rocks to the southwest and Paleozoic–Mesozoic granitoid–greenstone terranes to the northeast. Auriferous quartz veins are the dominant ore type and are spatially associated with widespread hydrothermal alteration (Miao et al., 2005; Deng et al., 2009a, 2014b).

The Xiaoqinling–Xiong'ershan region, the second largest gold-producing district in China, with an indicated resource of 425 t Au for the Xiaoqinling area and about 300 t Au for the Xiong'ershan area, is located on the southern margin of the NCC, north of the Qinling–Dabie Orogenic Belt (Fig. 1; Mao et al., 2002; Zhou et al., 2014; Li et al., 2015). Gold deposits in the Xiaoqinling area are mostly hosted in Neoarchean amphibolite-facies metamorphic rocks, with a few smaller deposits in the Mesozoic plutons. They are controlled by NW-trending brittle to brittle-ductile faults. The orebodies consist of auriferous quartz veins and subordinate disseminated ores in proximal alteration zones (Li et al., 2012). Gold deposits in the central part of the Xiong'ershan area are mainly hosted in Precambrian metamorphic rocks with subordinate deposits on the margin of Mesozoic plutons. Ore styles include auriferous quartz veins, disseminated gold in altered rocks, and Cretaceous gold-bearing volcanic breccia pipes (Mao et al., 2002).

The northern margin of the NCC is well endowed with non-ferrous metals as well as gold. Two main gold districts, Daqinshan and Yan-Liao, are defined (Fig. 1). About 70% of the gold resource is hosted in high-grade Archean and Paleoproterozoic metamorphic rocks and the remainder in late Paleozoic to Mesozoic granitoids. Gold mineralization is dominated by low-sulfide, gold-bearing quartz veins, and minor disseminated gold in altered rocks and tectonic breccias (Hart et al., 2002; Wang et al., 2012).

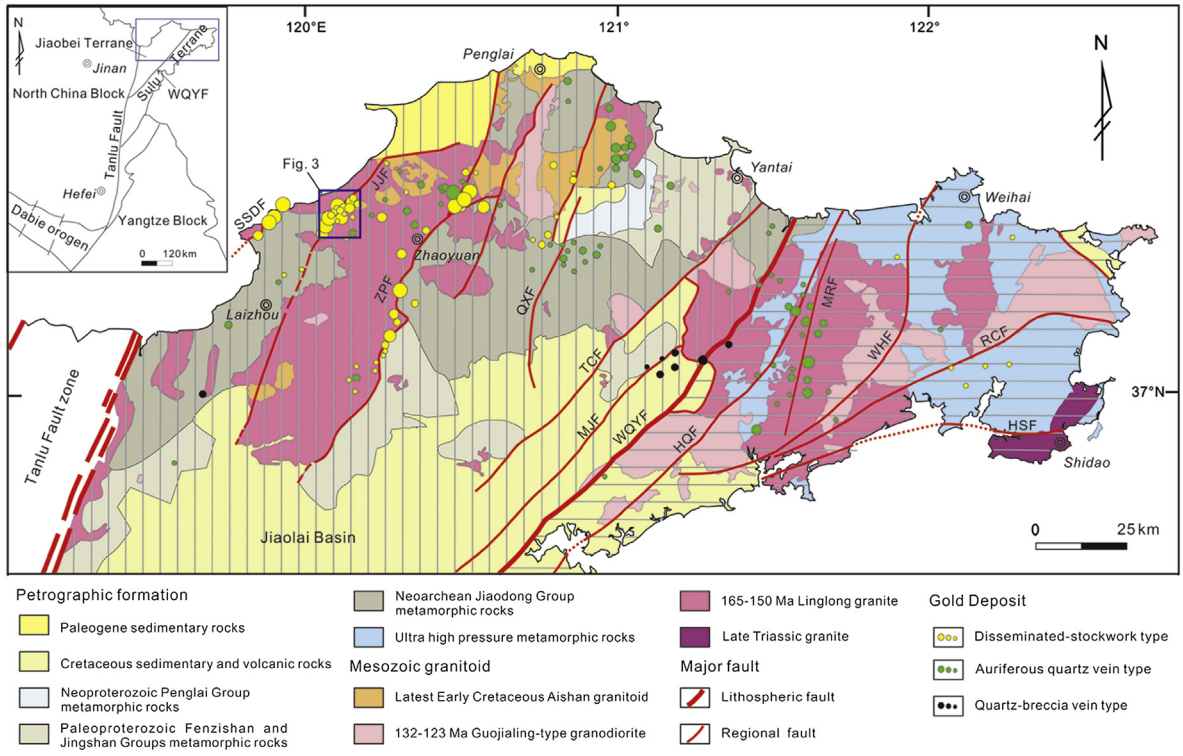

Figure 2. Simplified geological map of the Jiaodong gold province showing the distribution of major fault zones, Precambrian metamorphic rocks, Mesozoic granitoid intrusions, sedimentary rocks and gold deposits (after Yang et al., 2014a). Different size circles represent gold tonnages of the gold deposits (>100 t, 100–50 t, 50–20 t, 20–5 t, 5–1 t), respectively. The Jiaojia gold field is situated at the northwestern part of the Jiaodong Peninsula. HQF: Haiyang–Qingdao Fault; HSF: Haiyang–Shidao Fault; JJF: Jiaojia Fault; MJF: Muping–Jimo Fault; MRF: Muping–Rushan Fault; QXF: Qixia Fault; RCF: Rongcheng Fault; SSDF: Sanshandao Fault; TCF: Taocun Fault; WHF: Weihai Fault; WQYF: Wulian–Qingdao–Yantai Fault; ZPF: Zhaoping Fault.

3. Mineral district geology

The Xincheng gold deposit is situated in the northwestern part of the Jiaodong Peninsula, where it is underlain by two Precambrian tectonic units, the Jiaobei Terrane in the northwest and the Sulu Terrane in the southeast (Fig. 2). The Jiaobei Terrane comprises the Jiaobei Uplift in the north and the Jiaolai Basin in the south. The former has by far the largest gold endowment, including more than 90% of the proven gold resources (~3600 t Au; Yang et al., 2014a) and the vast majority of world-class to giant gold deposits in the Jiaodong gold province. It is dominated by Precambrian metamorphic basement and supracrustal rocks cut by Mesozoic intrusions (Fig. 2).

The Precambrian basement includes the Neoarchean Jiaodong Group amphibolite and mafic granulite sequence, and Archean (2.9–1.9 Ga) TTG gneisses (Tang et al., 2007, 2008; Jahn et al., 2008; Geng et al., 2012), the Paleoproterozoic Fenzishan Group schist, paragneiss, calc-silicate rocks, marble, and minor mafic granulite and amphibolite (Dong et al., 2010; Li et al., 2013; Liu et al., 2013), and the Neoproterozoic Penglai Group marble, slate and quartzite (Faure et al., 2004).

The intrusions are of late Jurassic, middle–early Cretaceous and late–early Cretaceous age. The late Jurassic calc-alkaline granites, dated at 165–150 Ma (Zhang et al., 2010; Ma et al., 2013), are batholiths comprising biotite-monzogranite, monzodiorite, quartz-diorite and granodiorite. The magma was derived from partially melted Neoarchean lower crust with intrusions emplaced at a depth of 25–30 km (Zen and Hammarstrom, 1984; Chen et al., 1996). The middle–early Cretaceous potassic calc-alkaline granites, dated at 132–123 Ma (Liu et al., 2014; L. Wang et al., 2014), mainly include the Sanshandao, Shangzhuang, Beijie, Congjia and Guojialing granites, varying from granite to granodiorite and alkaline rock from west to east. The magma derived from both delaminated eclogitic lower crust and upwelling asthenospheric mantle (Hou et al., 2007) with intrusion depths of 5–13 km (Chen et al., 1993; Lin and Yin, 1998). The late–early Cretaceous alkaline granites and potassic mafic dikes are dated at 125–90 Ma (Guo et al., 2005; Zhang and Zhang, 2007).

An E- to W-trending fold belt formed during Triassic collision between the North China Craton and the South China Craton (Zhang et al., 2007). NE- to NNE-trending faults control most of the gold deposits and are thought to be secondary faults related to the Tan–Lu Fault (Deng et al., 2008, 2009b, 2011; Yang et al., 2014b). They are distributed at intervals of 35 km from west to east as the Sanshandao, Jiaojia, Zhaoping and Qixia Faults (Deng et al., 2006). NW-trending faults dip NE or SW at 60°–80° and commonly cut the NE- to NNE-trending faults (Deng et al., 1996, 2010).

4. Deposit geology

The Xincheng gold deposit (37°25′45″–37°27′01″N, 120°07′28″–120°08′58″E) is one of the largest gold deposits in Jiaodong with a proven resource of >200 t Au, including 80.68 t Au that has already been produced. It has been exploited since 1979 by the Xincheng Gold Company, with an estimated annual production of 5.37 t gold in 2013. The Xincheng gold deposit, occupying an area of 3.91 km^2, is located about 35 km northeast of Laizhou City in the northwestern part of the Jiaobei Uplift, and near the northern extremity of the Jiaojia gold field, which has proven gold resources of >1200 t (Deng et al., 2015; Fig. 3). The granitoids, which account for 90% of the outcrop area, are widely distributed in the Xincheng gold deposit. The Xincheng granitoids, with a zircon LA-ICP-MS age of ca. 132–123 Ma (Liu et al., 2014; L. Wang et al., 2014), occur as a NE-trending stock intruding the Linglong granitic pluton, and consist of quartz monzonite and monzogranite, which host the ore deposit.

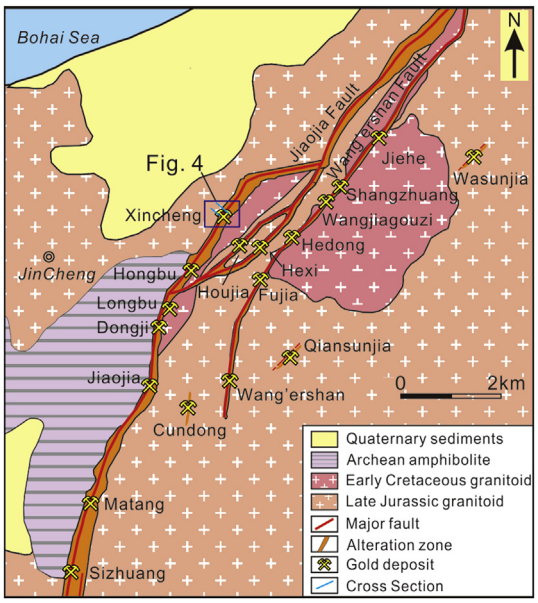

Figure 3. Simplified geological map of the Jiaojia Fault zone showing the distribution of major structures and representative gold deposits (modified from Wang et al., 2015; Wei et al., 2015).

The greyish-green to charcoal-grey quartz monzonite, which constitutes the central part of the pluton, has a medium- to fine-grained granular texture, whereas, towards its margins, grain size progressively increases and the rock becomes a light flesh-pink medium- to coarse-grained and medium- to fine-grained porphyritic monzogranite (L. Wang et al., 2014). The diffuse boundary between these varieties of monzonite to monzogranite (Fig. 3) implies that they are coeval intrusions (Liu et al., 2014). Jiaodong Group enclaves have diffuse boundaries with the quartz monzonite in the hangingwall of the Jiaojia Fault. Thin NE-trending mafic to felsic dikes, which are rare in the monzogranite, intrude the quartz monzonite (Fig. 3).

The ore zones, comprising two mineralization styles, are structurally controlled by the NE-trending and NW-dipping Jiaojia Fault and subsidiary faults, and are mainly restricted to the granitoids in the footwall of the fault (Figs. 3 and 4). The more common mineralization type, which contains the bulk of the gold resources, comprises disseminated- and stockwork-style ores within altered granitoids, and is characterized by strong sericitization, silicification, sulfidation and K-feldspar wallrock alteration halos, together with minor carbonate alteration. Both ores and halos are controlled by the structural heterogeneities in the Jiaojia Fault zone, and are located in the principal displacement faults at divergent bends and dilational jogs and/or subsidiary structures such as intersecting faults (Fig. 4). Fault zones contain hydrothermal breccias and cataclastic rocks, which comprise up to 50 m thick zones of K-feldspar, quartz, and sericite with both disseminated pyrite and pyrite–quartz stockworks (Qiu et al., 2002), reflecting mostly brittle failure and contemporaneous fluid flow. Another less-common ore type comprises a series of *en-echelon* auriferous quartz–pyrite veins, that are controlled by the NE- and NNE-trending subsidiary faults which cut the granitoids (Fig. 4).

Based on cross-cutting relationships and mineral paragenesis, four mineralization stages are recognized in the Xincheng lode systems (Fig. 5). These are pyrite–quartz–sericite (stage 1), quartz–pyrite (stage 2), quartz–polysulfide (stage 3) and quartz–carbonate (stage 4). Multiple types of hydrothermal alteration are recorded at Xincheng, including sericitization, silicification,

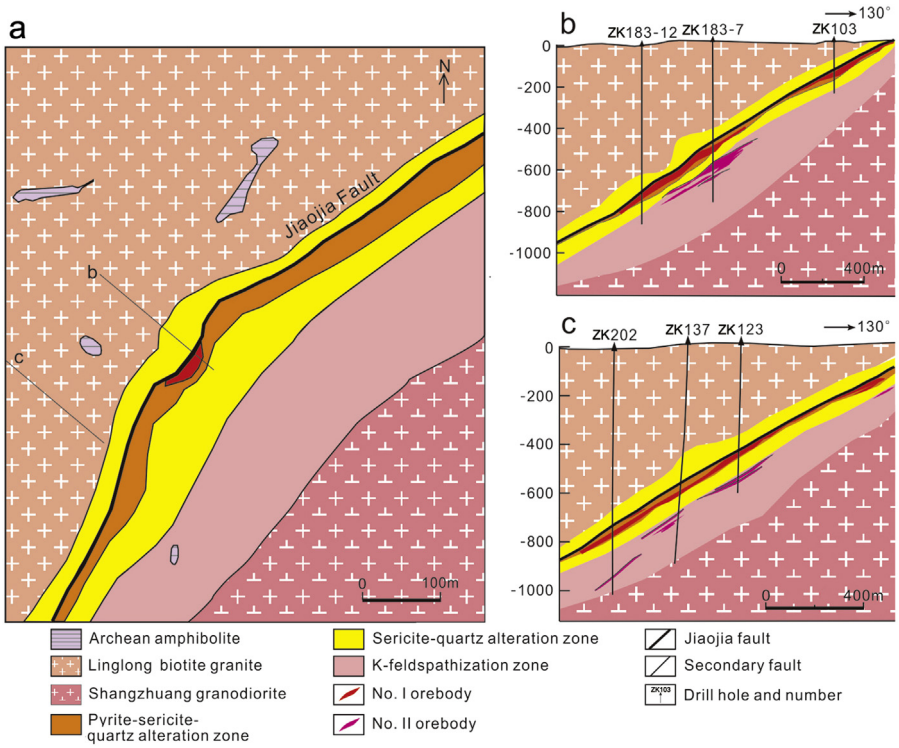

Figure 4. Sketch map of the orebody and fault zone at the Xincheng gold deposit, showing the structural controls of the Jiaojia Fault on mineralization and hydrothermal alteration. (a) Plan view of Xincheng; (b and c) schematic vertical cross-sections along lines b and c.

sulfidation, carbonation and K-feldspathization, which are largely restricted to fault zones (Fig. 4). Sericitization is characterized by the partial or complete replacement of plagioclase, K-feldspar or biotite with fine-grained sericite, and accompanied by fine-grained quartz and minor pyrite. Following sericite–quartz alteration, abundant sulfide minerals were precipitated to form quartz–pyrite and quartz–polymetallic sulfides veinlets, which are rarely cut by carbonate (–quartz) veinlets. These first alteration types are associated with the gold-forming event. K-feldspar fragments commonly occur in quartz–sericite–pyrite altered rocks, particularly near the Jiaojia Fault. This suggests that K-feldspathization was earlier than the hydrothermal events related to gold mineralization, although some workers regard K-feldspar to be the alteration mineral produced in stage 1 (Fan et al., 2003). In summary, the alteration minerals related to stage 1 are sericite and quartz, those related to stages 2 and 3 are chiefly quartz, with minor sericite, and those associated with stage 4 are quartz and calcite. These assemblages are broadly consistent with temperatures and pressures of mineral formation during the hydrothermal alteration at Xincheng of 225–400 °C and 100–300 MPa, respectively (McCuaig and Kerrich, 1998).

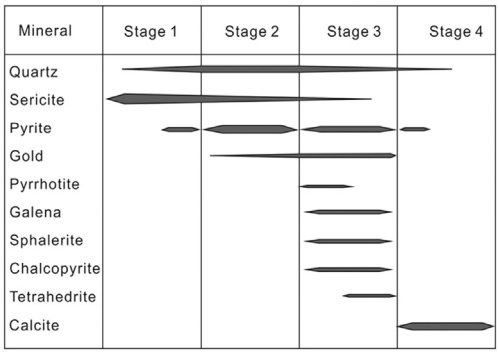

Figure 5. Paragenesis of gangue and ore minerals at the Xincheng deposit. Line thickness represents relative amount of the mineral.

5. Nature of orebodies

The No. I and No. II orebodies, which comprise 98.6% of the proven reserves in the Xincheng deposit, are located in the footwall of the Jiaojia Fault and the secondary faults, respectively, as described below (Fig. 4).

The No. I orebody, the largest orebody (reserves of about 185 t Au), is characterized by disseminated- and stockwork-style ores (Fig. 4). The orebody is about 200 m long, with a strike of 37° and dip of 26°–40° to the northwest. It ranges in thickness from 0.8 to 55 m (average 18.21 m), and extends down dip from the 30 m level to below the –1000 m level, with a barren section between the –250 to –450 m levels. The gold grade varies from 3.28 to 20.37 g/t Au with an average of 7.34 g/t Au.

The No. II orebody, with about 15 t gold, is mainly in the footwall of the No. I orebody (Fig. 4). It is characterized by quartz–pyrite and quartz–sulfide vein-style ores, and comprises a series of subparallel veins filling subsidiary, NE- to NEE-trending faults. It forms S-shape, stratiform-like lenses that strike 31° and dip 50–60°NW, ranging in thickness from 0.5 to 20 m with an average of 6.57 m. The gold grade varies from 3 to 40 g/t Au with an average of 8.70 g/t Au.

Microscope and SEM observations and EPMA results show that gold occurs dominantly as electrum (Au, 37.02–77.33%; Ag, 22.36–59.00%), with lesser amounts of native gold (Au, 82.82–98.58%; Ag, 0.02–14.62%) and rare native silver and argentite, normally associated with pyrite, chalcopyrite, galena and sphalerite. The three types of visible gold are inclusions in sulfides, microveinlets in cracks in sulfides and grains on the margins of

sulfide crystals, mainly pyrite and chalcopyrite. Electrum is dominantly hosted as inclusions in, or fracture filling of, pyrite and quartz. The distribution and grade of gold are controlled by fractures in sulfides and quartz associated with ductile–brittle deformation.

The main ore components are gold and silver, with subordinate copper and sulfur. Silver is the main byproduct, with proven resources of ~105 t, and grade of 1.28–19.56 g/t silver (average 3.74 g/t). Sulfur is the second most important byproduct, with proven resources of 5100 t, and a grade of 0.10–2.85% sulfur (average 1.13%, locally >2%). Copper has proven resources of 713 t, and grade of 0.0006–0.032% copper (average 0.004%). The grades of deleterious components are low (Pb = 0.0068%, Zn = 0.0051%, As = 2.73 g/t), and do not affect the separation of minerals and the metallurgical operation.

6. Ore and ore-fluid geochemistry

6.1. Fluid inclusion data

Previous fluid inclusion studies showed that ore fluids have temperature-pressure P–T conditions of 170–330 °C and 50–269 MPa (Hu et al., 2005, 2007; Yang et al., 2007, 2009; Cai et al., 2011), H_2O–CO_2 ± CH_4 fluid chemistry, with low to moderately salinity (1.2–13.6 wt.% NaCl eq.), for both the Jiaojia- and Linglong-style gold deposits in Jiaodong (Fan et al., 2010). Furthermore, Lu et al. (2011), L. Wang et al. (2014) and Wang et al. (2014a,b) reported that gold-related CO_2-rich and aqueous inclusions have similar homogenization temperatures in the Xincheng gold deposit. Three types of ore-related fluid inclusions have been identified through a recent systemic petrography, microthermometry, and Raman spectroscopy study (Wang et al., 2015). Type 1 aqueous–carbonate (H_2O–CO_2) inclusions generally are 4–10 μm in diameter, and appear as clusters or along pseudosecondary trails, with temperatures of total homogenization of 221–304 °C (average 261 ± 19 °C; 1σ; n = 101) (Table 1; Fig. 6). The CO_2 volumetric proportion is 20–50% in both two- (liquid H_2O + CO_2-rich vapor) and three-phase (liquid H_2O + liquid CO_2 + CO_2-rich vapor) inclusions. Type 2 aqueous inclusions (liquid H_2O + vapor H_2O) are normally small (2–7 μm), and exist in clusters and along pseudosecondary trails, coexisting with type 1 inclusions. Homogenization of the liquid phase occurred between 171 and 264 °C (average 224 ± 22 °C; 1σ; n = 35) (Table 1; Fig. 6). Type 3 CO_2 inclusions (liquid CO_2 and vapor CO_2) are generally small (2–6 μm), and distributed within CO_2–H_2O inclusion clusters.

Calculated salinities in type 1 inclusions are 2.4–8.9 wt.% NaCl eq., and 3.1–13.3 wt.% NaCl eq. for type 2 inclusions. Bulk densities of type 1 inclusions vary from 0.858 to 1.022 g/cm^3, and 0.681 to 0.751 g/cm^3 for type 3 inclusions.

These results show that fluid immiscibility played an important role in gold mineralization at Xincheng. The pressure conditions of this immiscibility are estimated to vary between 78 and 208 MPa from isochore calculations at the trapping temperatures of 261 ± 19 °C (Fig. 7; Wang et al., 2015).

6.2. Isotope geochemistry

6.2.1. $\delta^{34}S$ isotope compositions of pyrite

Many sulfur, hydrogen, and oxygen isotope measurements have been carried out on ore-related minerals in the Xincheng gold deposit (Zhang, 1985, 1989; Luo and Miao, 2002; Lu et al., 2011; L. Wang et al., 2014; Wang et al., 2014a,b; Zhang et al., 2014; Tables 2 and 3). The $\delta^{34}S_{CDT}$ values of hydrothermal sulfides have a narrow range of 4.3–10.6‰ (n = 79; Fig. 8a). The $\delta^{34}S$ values of stage 1 pyrite are 6.5–10.6‰ (n = 15); stage 2 pyrite, 5.7–10.6‰

Table 1
Summary of the microthermometric data and composition of fluid inclusions trapped in quartz from veins and breccias at the Xincheng gold deposit (modified from Wang et al., 2015).

Sample	Fluid inclusion type	$T_{h,TOT}$ (°C)	wt.% NaCl eq.	Bulk X_{H_2O}	Bulk X_{NaCl}	Bulk $X_{CO_2+CH_4}$	Carbonic X_{CO_2}	Carbonic X_{CH_4}	Bulk density	Bulk molar volume
XC10D207B4	Type 1	235–304	5.41–8.45	0.796–0.917	0.016–0.024	0.061–0.185	0.920–0.990	0.010–0.080	0.858–0.997	20.63–26.24
quartz-pyrite veins	aqueous-carbonic									
	Type 2 aqueous	217–249	3.85–13.33	0.955–0.988	0.012–0.045				0.837–0.928	21.12–22.10
	Type 3 carbonic	22.7–26.5					1.000	0.000	0.710–0.751	58.63–62.03
XC10D215B1	Type 1	238–296	2.42–8.45	0.777–0.931	0.014–0.025	0.053–0.203	0.965–0.990	0.010–0.035	0.890–0.993	20.58–27.06
quartz-pyrite veins	aqueous-carbonic									
	Type 2 aqueous	171–248	3.69–7.29	0.976–0.988	0.012–0.024				0.856–0.939	19.96–22.04
	Type 3 carbonic	27.1–28.8					1.000	0.000	0.681–0.702	62.66–64.64
XC10D007B2	Type 1	221–282	2.42–7.14	0.804–0.926	0.013–0.022	0.058–0.180	0.885–0.965	0.035–0.115	0.898–0.999	20.36–24.93
quartz-pyrite veins	aqueous-carbonic									
	Type 2 aqueous	218–241	5.70–7.44	0.976–0.982	0.018–0.024				0.862–0.900	21.10–21.81
XC10D210B13	Type 1	252–295	4.14–8.77	0.829–0.941	0.012–0.025	0.042–0.146	0.895–1.000	0.000–0.105	0.926–1.005	19.93–24.58
quartz-polysulfide veins	aqueous-carbonic									
	Type 2 aqueous	209–264	3.05–10.24	0.966–0.990	0.010–0.034				0.798–0.932	20.79–23.06
XC10D206B10	Type 1	235–298	3.57–8.93	0.883–0.950	0.011–0.028	0.033–0.105	0.920–0.990	0.010–0.080	0.934–1.020	19.25–22.71
quartz-polysulfide veins	aqueous-carbonic									
	Type 2 aqueous	210–247	4.79–9.73	0.968–0.985	0.015–0.032				0.858–0.902	20.96–22.03
XC11D006B2	Type 1	225–279	4.69–7.81	0.800–0.936	0.014–0.023	0.046–0.186	0.925–0.985	0.015–0.075	0.912–1.022	19.66–25.69
quartz-polysulfide veins	aqueous-carbonic									
	Type 2 aqueous	174–232	4.48–11.47	0.962–0.986	0.014–0.038				0.893–0.929	20.03–21.46
	Type 3 carbonic	23.3–28.4					1.000	0.000	0.686–0.745	59.11–64.15

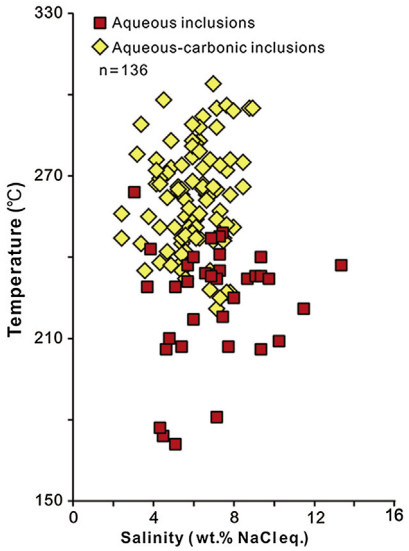

Figure 6. Temperatures (°C) of total homogenization ($T_{h,TOT}$) versus salinity (wt.% NaCl eq.) for type 1 aqueous–carbonic and type 2 aqueous inclusions (data from Table 1).

($n = 20$); stage 3 pyrite, 4.3–9.4‰ ($n = 28$); and stage unknown pyrite, 8.5–10.5‰ ($n = 16$).

There is no obvious difference between $\delta^{34}S$ values of each stage, indicating that they most likely came from the same source. All of the $\delta^{34}S$ values are within the range of those from all the gold deposits in Jiaodong (Fig. 8b; Yang et al., 2014a and the references therein) and also have similar ranges to the whole-rocks and sulfides from the Archean Jiaodong Group and Proterozoic Jingshan Group, and magmatic pyrite from the Mesozoic Linglong and Guojialing granitoid and intermediate–basic dikes (Fig. 8). Considering that the $\delta^{34}S$ values are greater than zero, a mantle-derived source can be excluded. Even though the average $\delta^{34}S$ value for the Xincheng gold deposit approaches that of the Guojialing granitoid, it is not possible to establish whether the ore-forming fluids had a magmatic or metamorphic source on the basis of the sulfur isotopes alone.

6.2.2. $\delta^{18}O$ and δD of quartz and fluids

The $\delta^{18}O$ values of hydrothermal quartz [$\delta^{18}O_{SMOW}$ (‰)] range from 8.0 to 16.7‰ (mainly 9.8–13.9‰) with a median value of

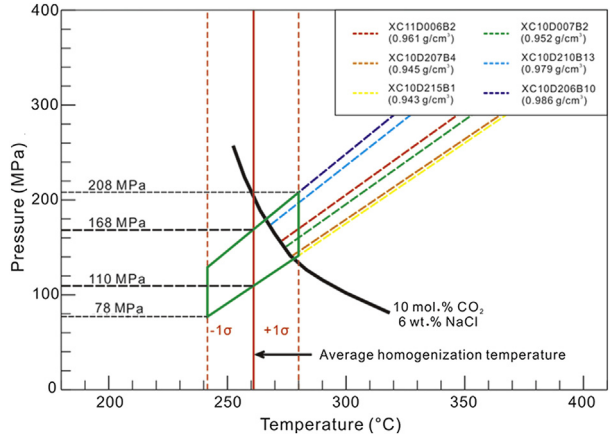

Figure 7. Representative isochors calculated for H_2O–CO_2 inclusions and the solvus for H_2O–CO_2 fluids. Green box shows the P–T window calculated according to the 1σ standard deviation homogenization temperature range (after Wang et al., 2015).

Table 2
Sulfur isotope compositions for sulfides from the four mineralization stages at the Xincheng gold deposit.

Stage	Mineral	$\delta^{34}S_{CDT}$ (‰)	References
1	Pyrite	9.8	Zhang et al., 2014
1	Pyrite	9.2	Zhang et al., 2014
1	Pyrite	9.9	Zhang et al., 2014
1	Pyrite	9.5	Zhang et al., 2014
1	Pyrite	10.5	Zhang et al., 2014
1	Pyrite	10.6	Zhang et al., 2014
1	Pyrite	10.5	Zhang et al., 2014
1	Pyrite	8.4	Zhang et al., 2014
1	Pyrite	9.9	Zhang et al., 2014
1	Pyrite	8.8	Zhang et al., 2014
1	Pyrite	8.7	Lu et al., 2011
1	Pyrite	6.5–8.4 ($n = 4$)	Wang, 2012
2	Pyrite	8.5	Zhang et al., 2014
2	Pyrite	8.3	Zhang et al., 2014
2	Pyrite	8.9	Zhang et al., 2014
2	Pyrite	9.1	Zhang et al., 2014
2	Pyrite	8.7	Zhang et al., 2014
2	Pyrite	9.7	Zhang et al., 2014
2	Pyrite	7.7	Zhang et al., 2014
2	Pyrite	8.3	Zhang et al., 2014
2	Pyrite	8.5	Lu et al., 2011
2	Pyrite	9.3	Lu et al., 2011
2	Pyrite	10.6	Lu et al., 2011
2	Pyrite	9.8	Lu et al., 2011
2	Pyrite	5.7–9.4 ($n = 8$)	Wang, 2012
3	Pyrite	8.2	Zhang et al., 2014
3	Pyrite	9.4	Zhang et al., 2014
3	Pyrite	7.6	Zhang et al., 2014
3	Sphalerite	7.9	Zhang et al., 2014
3	Galena	5.7	Zhang et al., 2014
3	Pyrite	8	Zhang et al., 2014
3	Pyrite	5.7	Zhang et al., 2014
3	Sphalerite	8.1	Zhang et al., 2014
3	Pyrite	7	Zhang et al., 2014
3	Galena	4.3	Zhang et al., 2014
3	Pyrite	6.7	Zhang et al., 2014
3	Chalcopyrite	5.8	Zhang et al., 2014
3	Pyrite	7.5	Zhang et al., 2014
3	Sphalerite	7.7	Zhang et al., 2014
3	Pyrite	6.9	Zhang et al., 2014
3	Pyrite	6.7–9.2 ($n = 13$)	Wang, 2012
unknown	Pyrite	8.0–9.5 ($n = 3$)	Wang, 2012
unknown	sulfide	9.5–10.5 ($n = 12$)	No. 6 Geological Team of Shandong Bureau, 1:25000 gold mineralization report, 1993
unknown	pyrite	10.1	Lu et al., 1999

13.0‰. The δD values of fluid inclusions [δD_{SMOW} (‰)] in hydrothermal quartz range from −96 to −61‰, with a median value of −75‰ (Table 3). The quartz in the four stages is probably the same, because of the similar median $\delta^{18}O$ values of hydrothermal quartz for each stage (12.2‰ → 13.9‰ → 10.0‰ → 10.7‰). The δD values of fluid inclusions in the quartz range from −96‰ to −61‰, with nearly constant median values for each stage (−73‰ → −79‰ → −72‰ → −86‰). The almost constant $\delta^{18}O$ and δD values indicate that the ore-forming fluids may be from the same continuous source. The calculated oxygen isotopic compositions of hydrothermal waters [$\delta^{18}O_{water}$ (‰)] have a wide range from −6.4 to 8.9‰ (Fig. 9), with the median values decreasing from 6.3‰, to 5.4‰, to 1.1‰, and to −5.7‰ in stages 1–4, respectively (Table 3). However, the decrease in the calculated $\delta^{18}O$ values with decline in the estimated equilibrium temperatures (330, 260, 250 and 140 °C for each stage) does not accord with the real trapping

Table 3
Hydrogen and oxygen isotope compositions for quartz and hydrothermal fluids from the four mineralization stages at the Xincheng gold deposit.

Stage	Mineral	δD_{SMOW} (‰)	$\delta^{18}O_{SMOW}$ (‰)	$\delta^{18}O_{water}$ (‰)	References
1	Quartz	−76	12.9	7.0	Lu et al., 2011
1	Quartz	−61	12.6	6.7	L. Wang et al., 2014; Wang et al., 2014a,b
1	Quartz	−69	11.7	5.8	L. Wang et al., 2014; Wang et al., 2014a,b
1	Quartz	−75	12.7	6.8	L. Wang et al., 2014; Wang et al., 2014a,b
1	Quartz	−72	11.1	5.2	Wang, 2012
1	Quartz	−67	14.8	8.9	Wang, 2012
1	Quartz	−82	10.3	4.4	Wang, 2012
1	Quartz	−88	11.8	5.9	Wang, 2012
2	Quartz	−91	13.5	5.0	Luo and Miao, 2002
2	Quartz	−81	14.7	6.2	Zhang, 1989
2	Quartz	−89	13.9	5.4	Zhang, 1989
2	Quartz	−82	12.8	4.3	Lu et al., 2011
2	Quartz	−68	13.3	4.8	L. Wang et al., 2014; Wang et al., 2014a,b
2	Quartz	−77	13.6	5.1	Wang, 2012
2	Quartz	−87	13.9	5.4	Wang, 2012
2	Quartz	−67	12.1	3.6	Wang, 2012
2	Quartz	−73	14.4	5.9	Wang, 2012
2	Quartz	−75	13.7	5.2	Wang, 2012
2	Quartz	−69	15.3	6.8	Wang, 2012
2	Quartz	−72	13.7	5.2	Wang, 2012
2	Quartz	−70	16.7	8.2	Wang, 2012
2	Quartz	−74	13.8	5.3	Wang, 2012
2	Quartz	−93	14.4	5.9	Wang, 2012
2	Quartz	−82	15.2	6.7	Wang, 2012
2	Quartz	−86	13.9	5.4	Wang, 2012
2	Quartz	−96	15.7	7.2	Wang, 2012
3	Quartz	−70	11.4	2.5	Wang, 2012
3	Quartz	−70	10.0	1.1	Wang, 2012
3	Quartz	−72	13.0	4.1	Wang, 2012
3	Quartz	−82	8.0	−0.9	Wang, 2012
3	Quartz	−70	10.9	2.0	Wang, 2012
3	Quartz	−73	9.8	0.9	Wang, 2012
3	Quartz	−95	8.7	−0.2	Wang, 2012
4	Quartz	−86	10.0	−6.4	Wang, 2012
4	Quartz	−87	11.4	−5.0	Wang, 2012

Notes: $\delta^{18}O_{water}$ (‰) is calculated by $\delta^{18}O_{SMOW}$ (‰) with the equation: $\delta^{18}O_{water} = \delta^{18}O_{SMOW} - 3.38 \times 10^6 T^{-2} + 3.40$ (Clayton et al., 1972); equilibrium temperatures of stages 1–4 are 330, 260, 250 and 140 °C, respectively.

temperatures, indicating it is not credible. Considering that isotopic exchange occurred during water–rock reactions associated with large-scale hydrothermal alteration, the early-stage fluids should be closer to the primary fluids (Guo et al., 2014). Thus, the most

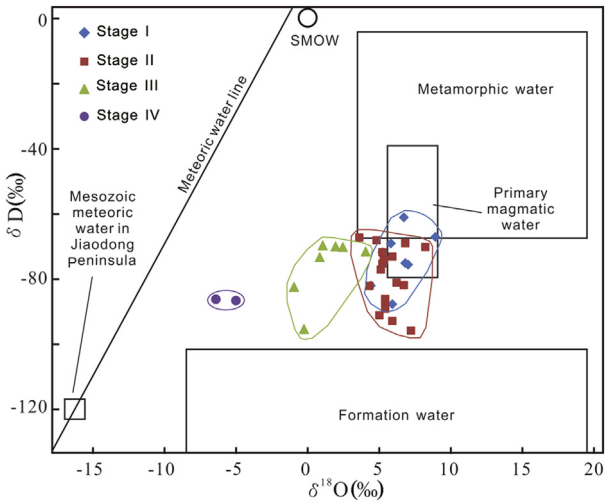

Figure 9. Calculated δD and $\delta^{18}O$ values of ore-forming fluids in the Xincheng gold deposit.

likely true $\delta^{18}O$ and δD compositions of the primary ore-forming fluid in the Xincheng gold deposit are stage 1 data (shown by the blue lines in Fig. 9).

Part of the data plot in the metamorphic water field, and the meteoric water and formation water can be easily dismissed according to the entirely different $\delta^{18}O$ and δD compositions. However, many generations of fluid inclusions (even post-mineralization fluid inclusions consisting of meteoric water) are trapped in quartz grains, which probably leads to the lower δD value calculated for the hydrothermal fluids. Thus, the true $\delta^{18}O$ and δD compositions should generally fall in the general fields of metamorphic water and primary magmatic water. However, in view of the low salinity (2.4–13.3 wt.% NaCl eq.) relative to the normally high-salinity magmatic–hydrothermal fluids (Rusk et al., 2008), ore-forming fluids in Xincheng are considered most likely to have had a metamorphic source.

6.3. Geochronology

Sericite/muscovite separates from ores and wallrock alteration of the Xincheng deposit yield $^{40}Ar/^{39}Ar$ ages of 120.7 ± 0.2 Ma to 120.2 ± 0.3 Ma (Li et al., 2003). The Rb–Sr isochron age of six pyrite-phyllic rock samples, from the main ores of the Xincheng gold deposit, is 116.6 ± 5.3 Ma with an initial $^{87}Sr/^{86}Sr$ value of 0.7113 ± 0.0006 and MSWD of 1.3 (Yang et al., 2000). Recent LA-

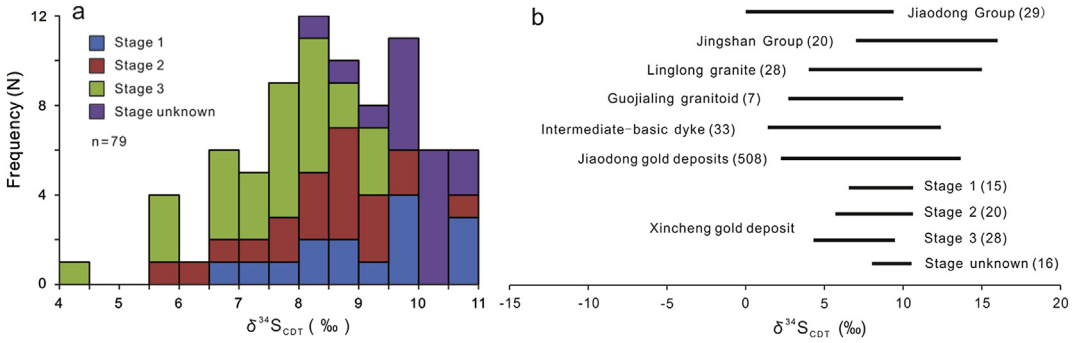

Figure 8. (a) Histograms of $\delta^{34}S$ values of hydrothermal pyrites from different stages at the Xincheng gold deposit; (b) comparison of sulfur isotopic compositions of the three mineralization stages at Xincheng and related major geologic bodies. The ranges of major geologic bodies are from Yang et al. (2014a).

ICP-MS zircon U–Pb study of the ore-hosting granodiorites suggests that they were emplaced at 123 ± 1 to 132 ± 1 Ma (Liu et al., 2014; L. Wang et al., 2014).

The $^{40}Ar/^{39}Ar$ age of sericite and muscovite is considered a relatively robust ore-formation age, because the grains are intimately associated with gold in the ores (Li et al., 2003). The LA-ICP-MS zircon U–Pb age of the ore-hosting granodiorites defines the earliest possible age of hydrothermal activity as they are the host to gold mineralization. Thus, the timing of gold mineralization at the Xincheng gold deposit is later than 123 ± 1 Ma, and is likely to be between 120.9 and 119.9 Ma.

7. A minerals system model

Much research has been conducted to define a minerals system model for the Jiaodong gold deposits, including Xincheng (Yang et al., 2007; Goldfarb and Santosh, 2014). Some workers have emphasized the importance of metamorphic fluids in ore formation (Yang et al., 2014a; Wang et al., 2015). Others have focused on the combination of meteoric and/or magmatic fluids during the mineralization process (Deng et al., 2003b; Fan et al., 2007; Mao et al., 2008). For example, Lu et al. (2011) reported that the ore fluids at the Xincheng gold deposit were low to moderate salinity (0.8–9.4 wt.% NaCl eq.), CO_2–H_2O–NaCl fluids, with a wide temperature range (147–380 °C). Combined with D–O–S isotope data, the ore fluids were interpreted to be originally magmatic fluids which mixed with meteoric water with fluid immiscibility possibly leading to gold precipitation (Lu et al., 2011). In contrast, L. Wang et al. (2014) and Wang et al. (2014a,b) indicated that the H_2O–CO_2 ore fluids are characterized by low salinity (2.1–10.2 wt.% NaCl eq.) and low density (0.54–0.97 g/cm^3) fluids, with limited temperature (260–300 °C) and pressure ranges (65–113 MPa). The δD_{water} and $\delta^{18}O$ values, ranging from −75.1 to −61.4‰ and 4.8 to 6.4‰, respectively, are best interpreted to indicate that the ore fluids of the Xincheng deposit are mainly from a deep metamorphic source (L. Wang et al., 2014; Wang et al., 2014a,b). Recent research shows that the initial ore-forming fluids belong to a medium temperature, CO_2-rich, and low salinity H_2O–CO_2 homogeneous system. Gold was most probably transported as a $Au(HS)_2^-$ complex in the hydrothermal solution that formed the orebody at Xincheng. Fluid immiscibility, due to unmixing from a single homogeneous H_2O–CO_2 parent fluid at P–T conditions of 221–304 °C and 78–208 MPa, is interpreted to have caused significant H_2S loss from the hydrothermal solution, thereby reducing $Au(HS)_2^-$ solubility with concomitant deposition of gold (Fig. 10; Wang et al., 2015).

The interpretation that a mantle-derived fluid is associated with the gold mineralization has commonly been supported by Ar and He isotope ratios for fluids extracted from inclusions in ore-bearing quartz veins (Zhang et al., 2002, 2008; Mao et al., 2008). However, these data only indicate the possible source of the Ar and He, but not the source of the major ore-forming fluids and the metals. The positive sulfur isotope values (Fig. 8) are also inconsistent with a mantle source for the sulfur. Similarly, the conclusion of meteoric water involvement is based on D–O isotopic data from the bulk extraction of fluid inclusions from quartz in the ores. As described above, such measurements are not definitive because the quartz contains both ore-related and post-mineralization fluid inclusions, and the low $\delta^{18}O$ values are due to a combination of isotopic exchange that occurred during water–rock reactions and underestimation of the real trapping temperatures.

Even though some orogenic gold deposits are interpreted to form as a result of a combination of metamorphic processes and magmatic inputs (Yardley and Cleverley, 2014), the low salinity (<13.3 wt.% NaCl eq.) fluid at Xincheng differs from normal high-salinity magmatic–hydrothermal fluids (Rusk et al., 2008). Furthermore, the alteration zoning and mineral composition in Xincheng are different from the gold deposit related to the magmatic hydrothermal solution. Thus, ore-forming fluids that formed the Xincheng gold deposit probably had a metamorphic source. The ore-forming fluids cannot be derived from the Neoarchean Jiaodong Group metamorphic rocks, because the gold event occurred about 2 Ga later than regional high-grade metamorphism. Combined with the geological and geochemical features described above, the most plausible likely fluid and metal reservoirs are those associated with the subducting Paleo-Pacific ocean slab (Goldfarb and Santosh, 2014).

As a result, it is possible to build a preferred minerals system model for the Xincheng deposit (Fig. 11). The initial ore-forming fluid is interpreted to have been a medium temperature, CO_2-rich, and low salinity H_2O–CO_2, deeply source metamorphic fluid, associated with the dehydration and decarbonization of the subducting Paleo-Pacific oceanic lithosphere and overlying oceanic sediment wedge. The brittle–ductile Jiaojia Fault constrained the advection of ore-forming fluids and metals. Fluid immiscibility, caused by episodic pressure drops, led to significant high-grade native gold deposition in the presence of limited sulfide deposition in the world-class Xincheng gold deposit.

However, our study of the texture and geochemistry of pyrite, combined with mesoscopic and microscopic observations at Xincheng, illustrated some significant differences from most orogenic gold deposits (Yang et al., 2016a). These include (1) the low

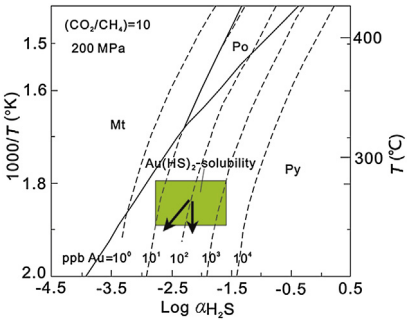

Figure 10. $Au(HS)_2^-$ solubility contours (dashed lines) as a function of temperature and H_2S content assuming an ore fluid with $CO_2/CH_4 = 10$, pH = 5.5 and P = 200 MPa, which approximates the physicochemical conditions of the hydrothermal systems responsible for deposition of the Xincheng deposit. Green box indicates the T–αH_2S conditions during gold mineralization at Xincheng. Vertical arrow marks a hypothetical fluid evolution path for the temperatures of ore fluids decreasing at constant fluid composition. Oblique arrow illustrates the ~10-fold decrease in $Au(HS)_2^-$ solubility that likely occurred during a moderate temperature and H_2S decrease in response to fluid immiscibility (after Mikucki, 1998).

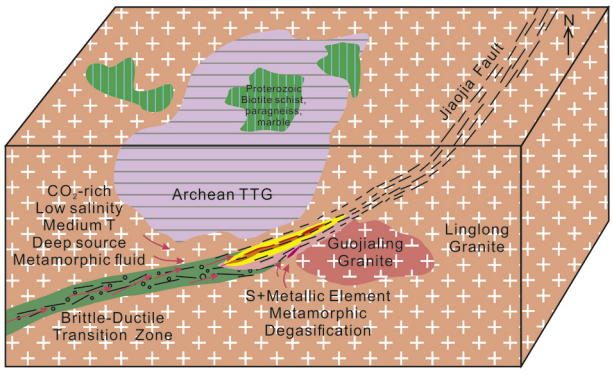

Figure 11. Suggested mineral system model for the Xincheng gold deposit.

concentrations of invisible gold in the relatively As-poor pyrite lattice compared to normally higher gold content in more As-rich pyrite in many orogenic gold deposits; (2) the pyrites contain about 20–100 times more Ag than Au, and the electrum has high Ag/Au ratios (0.3–1.6), which contrasts with most orogenic gold deposits, where the gold normally has less than 10% Ag (Groves et al., 1998; Goldfarb et al., 2005); (3) the appearance of galena and tellurobismuthite, indicating a relatively low ore-forming temperature; and (4) the dominantly brittle deformation textures in pyrite. Thus, the Xincheng deposit is interpreted to be an epizonal orogenic gold deposit in the sense of Groves et al. (1998) that formed at a relatively high crustal level from an advecting metamorphic fluid from a deep subcrustal source.

8. Summary

The Xincheng world-class gold deposit is located in the northwestern part of the giant Jiaodong gold province, in the southeast North China Craton. The ca. 120 Ma gold mineralization at Xincheng is likely to have been associated with regional lithosphere thinning, de-cratonization and large-scale magmatic activity during the late Jurassic to early Cretaceous. It is structurally controlled by the NE-trending and NW-dipping Jiaojia Fault and subsidiary faults, and hosted by ca. 132–123 Ma Xincheng quartz monzonites and monzogranites in the footwall of the fault. Gold occurrences are associated with sulfides, mainly pyrite, and form mainly disseminated- and stockwork-style ores in hydrothermal wallrock alteration halos.

A preferred minerals system model for the Xincheng deposit suggests an initial medium temperature, CO_2-rich, and low salinity H_2O–CO_2 deeply sourced metamorphic ore fluid associated with dehydration and decarbonization of subducting Paleo-Pacific oceanic lithosphere and overlying sulfidic sedimentary wedge. The Jiaojia Fault constrained the advection of ore-forming fluids and metals from deep crustal levels to higher levels at the brittle ductile transition. Fluid immiscibility, caused by episodic pressure drops, led to significant high-grade gold deposition in the world-class Xincheng gold deposit. Significant gold was deposited in dilational zones in faults, where episodic pressure drop and subsequent fluid immiscibility were enhanced to produce this epizonal orogenic gold deposit. Such fault jogs provide high-quality targets for additional large-tonnage gold ores hosted in late Mesozoic granitoids, both in the vicinity of Xincheng and in the giant orogenic gold province of the Jiaodong Peninsula generally.

Acknowledgments

We thank Prof. David Groves and Prof. Santosh for the invitation to prepare this paper for the Special Issue on Giant Mineral Deposits. Prof. David Groves and Prof. Richard J Goldfarb helped to greatly improve the manuscript. We thank Tony Cockbain for his assistance with English. This study was financially supported by the National Natural Science Foundation of China (Grant No. 41230311), the National Science and Technology Support Program (Grant No. 2011BAB04B09), the Geological Investigation Work Project of China Geological Survey (Grant No. 12120114034901) and 111 Project of China (Grant No. B07011).

References

Artemieva, I.M., Mooney, W.D., 2001. Thermal thickness and evolution of Precambrian lithosphere. Journal of Geophysical Research 106, 16387–16414.

Cai, Y.C., Fan, H.R., Hu, F.F., Yang, K.F., Lan, T.G., Yu, H., Liu, Y.M., 2011. Ore-forming fluids, stable isotope and mineralizing age of the Hubazhuang gold deposit, Jiaodong peninsula of eastern China. Acta Petrologica Sinica 27, 1341–1351 (in Chinese with English abstract).

Chen, G.Y., Sun, D.S., Zhou, X.R., Gong, R.T., Shao, Y., 1993. Mineralogy of Guojialing Granodiorite, its Relationship to Gold Mineralization in the Jiaodong Peninsula. Chinese University of Geosciences Press, Beijing, pp. 1–230 (in Chinese with English abstract).

Chen, G.Y., Sun, D.S., Shao, Y., 1996. Typomorphic significance of accessory minerals of gold-hosting Kunyushan monzonitic granite in Jiaodong, China. Geoscience 10, 175–186 (in Chinese with English abstract).

Chen, Y.J., Zhai, M.G., Jiang, S.Y., 2009. Significant achievements and open issues in study of orogenesis and metallogenesis surrounding the North China continent. Acta Geologica Sinica 25, 2695–2726 (in Chinese with English abstract).

Clayton, R.N., O'Neil, J.R., Mayeda, T.K., 1972. Oxygen isotope exchange between quartz and water. Journal of Geophysical Research 77, 3057–3067.

Deng, J., Xu, S.L., Fang, Y., Zhou, X.Q., Wan, L., 1996. Structural System, Gold Ore-forming Dynamics in the Northwestern Part of Jiaodong Peninsula. Geological Publishing House, Beijing, pp. 1–98 (in Chinese with English abstract).

Deng, J., Yang, L.Q., Sun, Z.S., 2003a. A metallogenic model of gold deposits of the Jiaodong granite-greenstone belt. Acta Geologica Sinica 77, 537–546 (in Chinese with English abstract).

Deng, J., Liu, W., Sun, Z.S., Wang, J.P., Wang, Q.F., Zhang, Q.X., Wei, Y.G., 2003b. Evidence of mantle-rooted fluids and multi-level circulation of ore-forming dynamics: a case study from the Xiadian gold deposit, Shandong Province, China. Science in China Series D: Earth Sciences 46, 138–142.

Deng, J., Yang, L.Q., Ge, L.S., Wang, Q.F., Zhang, J., Gao, B.F., Zhou, Y.H., Jiang, S.Q., 2006. Research advances in the Mesozoic tectonic regimes during the formation of Jiaodong ore cluster area. Progress in Natural Sciences 16, 513–518 (in Chinese with English abstract).

Deng, J., Wang, Q.F., Yang, L.Q., Zhou, L., Gong, Q.J., Yuan, W.M., Xu, H., Guo, C.Y., Liu, X.W., 2008. The structure of ore-controlling strain, stress fields in the Shangzhuang gold deposit in Shandong Province, China. Acta Geologica Sinica 82, 769–780 (in Chinese with English abstract).

Deng, J., Yang, L.Q., Gao, B.F., Sun, Z.S., Guo, C.Y., Wang, Q.F., Wang, P., 2009a. Fluid evolution and metallogenic dynamics during tectonic regime transition: example from the Jiapigou gold belt in Northeast China. Resource Geology 59, 140–152.

Deng, J., Wang, Q.F., Wan, L., Yang, L.Q., Gong, Q.J., Zhao, J., Liu, H., 2009b. Self-similar fractal analysis of gold mineralization of Dayingezhuang disseminated-veinlet deposit in Jiaodong gold province, China. Journal of Geochemical Exploration 102, 95–102.

Deng, J., Chen, Y.M., Liu, Q., Yang, L.Q., 2010. The Gold Metallogenic System, Mineral Resources Exploration of Sanshandao Fault Zone, Shandong Province. Geological Publishing House, Beijing, pp. 1–371 (in Chinese).

Deng, J., Wang, Q.F., Wan, L., Liu, H., Yang, L.Q., Zhang, J., 2011. A multifractal analysis of mineralization characteristics of the Dayingezhuang disseminated-veinlet gold deposit in the Jiaodong Gold Province of China. Ore Geology Reviews 40, 54–64.

Deng, J., Liu, X.F., Wang, Q.F., Pan, R.G., 2014a. Origin of the Jiaodong-type Xinli gold deposit, Jiaodong Peninsula, China: constraints from fluid inclusion and C–D–O–S–Sr isotope compositions. Ore Geology Reviews 65, 674–686.

Deng, J., Yuan, W.M., Carranza, E.J.M., Yang, L.Q., Wang, C.M., Yang, L.Y., Hao, N.N., 2014b. Geochronology and thermochronometry of the Jiapigou gold belt, northeastern China: new evidence for multiple episodes of mineralization. Journal of Asian Earth Sciences 89, 10–27.

Deng, J., Wang, C.M., Bagas, L., Carranza, E.J.M., Lu, Y.J., 2015. Cretaceous–Cenozoic tectonic history of the Jiaojia Fault and gold mineralization in the Jiaodong Peninsula, China: constraints from zircon U–Pb, illite K–Ar, and apatite fission track thermochronometry. Mineralium Deposita. http://dx.doi.org/10.1007/s00126-015-0584-1.

Dong, C.Y., Wang, S.J., Liu, D.Y., Wang, J.G., Xie, H.Q., Wang, W., Song, Z.Y., Wan, Y.S., 2010. Late Palaeoproterozoic crustal evolution of the North China Craton, formation time of the Jingshan Group: constraints from SHRIMP U-Pb zircon dating of meta-intermediate-basic intrusive rocks in eastern Shandong Province. Acta Petrologica Sinica 27, 1699–1706 (in Chinese with English abstract).

Dong, Y., Genser, J., Naebauer, F., Zhang, G., Liu, X., Yang, Z., Heberer, B., 2011. U–Pb and $^{40}Ar/^{39}Ar$ geochronological constraints on the exhumation history of the North Qingling terrane, China. Gondwana Research 19, 881–893.

Fan, H.R., Zhai, M.G., Xie, Y.H., Yang, J.H., 2003. Ore-forming fluids associated with granite-hosted gold mineralization at the Sanshandao deposit, Jiaodong gold province, China. Mineralium Deposita 38, 739–750.

Fan, H.R., Hu, F.F., Yang, J.H., Zhai, M.G., 2007. Fluid evolution and large-scale gold metallogeny during mesozoic tectonic transition in the Jiaodong Peninsula, Eastern China. Geological Society, Special Publications, London 280, 303–316.

Fan, H.R., Hu, F.F., Yang, K.F., Zhai, M.G., 2010. Gold ore-forming fluids and metallogeny in the Jiaodong Peninsula, Eastern China. Smart Science for Exploration and Mining 1–2, 219–221.

Faure, M., Lin, W., Monie, P., Bruguier, O., 2004. Paleoproterozoic arc magmatism, collision in Liaodong Peninsula (north-east China). Terra Nova 16, 75–80.

Geng, Y.S., Du, L.L., Ren, L.G., 2012. Growth, reworking of the early Precambrian continental crust in the North China Craton: constraints from zircon Hf isotopes. Gondwana Research 21, 517–529.

Goldfarb, R.J., Santosh, M., 2014. The dilemma of the Jiaodong gold deposits: are they unique? Geoscience Frontiers 5, 139–153.

Goldfarb, R.J., Taylor, R.D., Collins, G.S., Goryachev, N.A., Orlandinif, O.F., 2014. Phanerozoic continental growth and gold metallogeny of Asia. Gondwana Research 25, 48–102.

Goldfarb, R.J., Baker, T., Dube, B., Groves, D.I., Hart, C.J.R., Robert, F., Gosselin, P., 2005. Distribution, character, and genesis of gold deposits in metamorphic terranes. In: 100th Anniversary Volume of ECONOMIC GEOLOGY, pp. 407–450.

Groves, D.I., Santosh, M., 2015. Province-scale commonalities of some world-class gold deposits: implications for mineral exploration. Geoscience Frontiers 6 (3), 389–399.

Groves, D.I., Goldfarb, R.J., Gebre-Mariam, M., Hagemann, S.G., Robert, F., 1998. Orogenic gold deposits-a proposed classification in the context of their crustal distribution and relationship to other gold deposit types. Ore Geology Reviews 13, 7–27.

Guo, J.H., Chen, F.K., Zhang, X.M., Siebel, W., Zhai, M.G., 2005. Evolution of syn- to post-collisional magmatism from North Sulu UHP belt, eastern China: zircon U-Pb geochronology. Acta Petrologica Sinica 21, 1281–1301 (in Chinese with English abstract).

Guo, L.N., Zhang, C., Song, Y.Z., Chen, B.H., Zhou, Z., Zhang, B.L., Xu, X.L., Wang, Y.W., 2014. Hydrogen and oxygen isotopes geochemistry of the Wang'ershan gold deposit, Jiaodong. Acta Petrologica Sinica 30, 2481–2494 (in Chinese with English abstract).

Hart, C.J.R., Goldfarb, R.J., Qiu, Y.M., Snee, L., Miller, L.D., Miller, M.L., 2002. Gold deposits of the northern margin of the North China Craton: multiple late Paleozoic–Mesozoic mineralizing events. Mineralium Deposita 37, 326–351.

Hou, M.L., Jiang, Y.H., Jiang, S.Y., Ling, H.F., Zhao, K.D., 2007. Contrasting origins of Late Mesozoic adakitic granitoids from the northwestern Jiaodong Peninsula, East China: implications for crustal thickening to delamination. Geological Magazine 144, 619–631.

Hu, F.F., Fan, H.R., Shen, K., Zhai, M.G., Jin, C.W., Chen, X.S., 2005. Nature and evolution of ore-forming fluids in the Rushan lode gold deposit, Jiaodong peninsula of eastern China. Acta Petrologica Sinica 5, 1329–1338 (in Chinese with English abstract).

Hu, F.F., Fan, H.R., Yang, K.F., Shen, K., Zhai, M.G., Jin, C.W., 2007. Fluid inclusions in the Denggezhuang lode gold deposit at Muping, Jiaodong Peninsula. Acta Petrologica Sinica 9, 2155–2164 (in Chinese with English abstract).

Jahn, B.M., Liu, D.Y., Wan, Y.S., Song, B., Wu, J.S., 2008. Archean crustal evolution of the Jiaodong Peninsula, China, as revealed by zircon SHRIMP geochronology, elemental, Nd-isotope geochemistry. American Journal of Science 308, 232–269.

Li, S.R., Santosh, M., 2014. Metallogeny and craton destruction: records from the North China Craton. Ore Geology Reviews 56, 376–414.

Li, J.W., Vasconcelos, P.M., Zhang, J., Zhou, M.F., Zhang, X.J., Yang, F.H., 2003. $^{40}Ar/^{39}Ar$ constraints on a temporal link between gold mineralization, magmatism, and continental margin transtension in the Jiaodong gold province, eastern China. Journal of Geology 111, 741–751.

Li, J.W., Bi, S.J., Selby, D., Chen, L., Vasconcelos, P., Thiede, D., Zhou, M.F., Zhao, X.F., Li, Z.K., Qiu, H.N., 2012. Giant Mesozoic gold provinces related to the destruction of the North China craton. Earth and Planetary Science Letters 349–350, 26–37.

Li, X.P., Liu, Y., Guo, J.H., Li, H.K., Zhao, G.C., 2013. Petrogeochemical characteristics of the Paleoproterozoic high-pressure mafic granulite, calc-silicate from the Nanshankou of the Jiaobei terrane. Acta Petrologica Sinica 29, 2340–2352 (in Chinese with English abstract).

Li, X., Liu, Z.Y., Zhang, D.T., Chen, F., Zhao, K., 2015. Gold reserves predicting by the Qibofu law on the Xiaoqinling goldfield. The Earth 4, 157–159 (in Chinese).

Lin, W.W., Yin, X.L., 1998. The forming physicochemical conditions of Linglong granitic complex, its geological significance. Acta Geoscientia Sinica 19, 40–48 (in Chinese with English abstract).

Lin, W., Faure, M., Chen, Y., Ji, W.B., Wang, F., Wu, L., Charles, N., Wang, J., Wang, Q.C., 2013. Late Mesozoic compressional to extensional tectonics in the Yiwulüshan massif, NE China and its bearing on the evolution of the Yinshan–Yanshan orogenic belt Part I: structural analyses and geochronological constraints. Gondwana Research 23, 54–77.

Liu, G.P., Ai, Y.F., 2000. Studies on the mineralization age of Baiyun gold deposit in Liaoning. Acta Petrologica Sinica 16, 627–632 (in Chinese with English abstract).

Liu, P.H., Liu, F.L., Wang, F., Liu, J.H., Cai, J., 2013. Petrological, geochronological preliminary study of the Xiliu ~2.1Ga meta-gabbro from the Jiaobei terrane, the southern segment of the Jiao-Liao-Ji Belt in the North China Craton. Acta Petrologica Sinica 29, 2371–2390 (in Chinese with English abstract).

Liu, Y., Deng, J., Wang, Z.L., Zhang, L., Zhang, C., Liu, X.D., Zheng, X.L., Wang, X.D., 2014. Zircon U-Pb age, Lu-Hf isotopes, petrogeochemistry of the monzogranites from Xincheng gold deposit, northwestern Jiaodong Peninsula, China. Acta Petrologica Sinica 30, 2559–2573 (in Chinese with English abstract).

Lu, H.Z., Guha, J., Fang, G.B., 1999. Characteristics of ore-forming fluid in Linglong Gold Mine, Shandong, China. Geochimica 28, 421–437 (in Chinese with English abstract).

Lu, L.N., Fan, H.R., Hu, F.F., Yang, K.F., Zheng, X.L., Zhao, H., 2011. Ore-forming fluids and genesis of Xincheng altered rock gold deposit in northwestern Jiaodong Peninsula. Mineral Deposits 30, 522–532 (in Chinese with English abstract).

Luo, Z.K., Miao, L.C., 2002. Granite and Gold Deposit in Zhaoyuan-Laizhou Region, Jiaodong. Press of Metallurgy Industry, Beijing, pp. 1–157 (in Chinese).

Ma, L., Jiang, S.Y., Dai, B.Z., Jiang, Y.H., Hou, M.L., Pu, W., Xu, B., 2013. Multiple sources for the origin of Late Jurassic Linglong adakitic granite in the Shandong Peninsula, eastern China: zircon U–Pb geochronological, geochemical and Sr–Nd–Hf isotopic evidence. Lithos 162, 251–263.

Mao, J.W., Goldfarb, R.J., Zhang, Z.W., Xu, W.Y., Qiu, Y.M., Deng, J., 2002. Gold deposits in the Xiaoqinling-Xiong'ershan region, Qinling Mountains, central China. Mineralium Deposita 37, 306–325.

Mao, J.W., Wang, Y.T., Li, H.M., Pirajno, F., Zhang, C.Q., Wang, R.T., 2008. The relationship of mantle-derived fluids to gold metallogenesis in the Jiaodong Peninsula: evidence from D-O-C-S isotope systematic. Ore Geology Reviews 33, 361–381.

McCuaig, T.C., Kerrich, R., 1998. P-T-t-deformation-fluid characteristics of lode gold deposits: evidence from alteration systematics. Ore Geology Review 12, 381–453.

Miao, L.C., Qiu, Y.M., Fan, W.M., Zhang, F.Q., Zhai, M.G., 2005. Geology, geochronology, and tectonic setting of the Jiapigou gold deposits, southern Jilin Province, China. Ore Geology Reviews 26, 137–165.

Mikucki, E.J., 1998. Hydrothermal transport and depositional processes in Archean lode-gold systems: a review. Ore Geology Reviews 13, 307–321.

Qiu, Y.M., Groves, D.I., McNaughton, N.J., Wang, L.Z., Zhou, T.H., 2002. Nature, age and tectonic setting of granitoid-hosted orogenic gold deposits of the Jiaodong Peninsula, eastern North China craton, China. Mineralium Deposita 37, 283–305.

Rusk, B.G., Reed, M.H., Dilles, J.H., 2008. Fluid inclusion evidence for magmatic-hydrothermal fluid evolution in the porphyry copper-molybdenum deposit at Butte, Montana. Economic Geology 103, 307–334.

Tang, J., Zheng, Y.F., Wu, Y.B., Gong, B., Liu, X.M., 2007. Geochronology, geochemistry of metamorphic rocks in the Jiaobei terrane: constraints on its tectonic affinity in the Sulu orogeny. Precambrian Research 152, 48–82.

Tang, J., Zheng, Y.F., Wu, Y.B., Gong, B., Zha, X.P., Liu, X.M., 2008. Zircon U-Pb age, geochemical constraints on the tectonic affinity of the Jiaodong Terrane in the Sulu Orogen, China. Precambrian Research 161, 389–418.

Tang, H.S., Chen, Y.J., Santosh, M., Zhong, H., Wu, G., Lai, Y., 2013. C–O isotope geochemistry of the Dashiqiao magnesite belt, North China Craton: implications for the great oxidation event and ore genesis. Geological Journal 48, 467–483.

Wang, Z.L., 2012. Metallogenic System of Jiaojia Gold Field, Shandong Province, China. Ph.D. Thesis. China University of Geosciences, Beijing (in Chinese with English abstract).

Wang, C.H., Wang, D.H., Huang, F., Xu, J., Chen, Z.H., Ying, L.J., Liu, S.B., 2012. The major gold concentration areas in China and their resource potentials. Geology in China 39, 1125–1142 (in Chinese with English abstract).

Wang, L., Pan, Z.C., Sun, L.W., 2014. Fluid inclusions of the Xincheng gold deposit of Laizhou city in Shandong province. Journal of Jilin University: Earth Science Edition 44, 1166–1176 (in Chinese with English abstract).

Wang, Z.L., Yang, L.Q., Deng, J., Santosh, M., Zhang, H.F., Liu, Y., Li, R.H., Huang, T., Zheng, X.L., Zhao, H., 2014a. Gold-hosting high Ba-Sr granitoids in the Xincheng gold deposit, Jiaodong Peninsula, East China: petrogenesis, tectonic setting. Journal of Asian Earth Sciences 95, 274–299.

Wang, Z.L., Zhao, R.X., Zhang, Q., Lu, H.W., Li, J.L., Cheng, W., 2014b. Magma mixing for the high Ba-Sr Guojialing-type granitoids in Northwest Jiaodong Peninsula: constrains from petrogeochemistry and Sr-Nd isotopes. Acta Petrologica Sinica 30, 2595–2608 (in Chinese with English abstract).

Wang, Z.L., Yang, L.Q., Guo, L.N., Marsh, E., Wang, J.P., Liu, Y., Zhang, C., Li, R.H., Zhang, L., Zheng, X.L., Zhao, R.X., 2015. Fluid immiscibility and gold deposition in the Xincheng deposit, Jiaodong Peninsula, China: a fluid inclusion study. Ore Geology Reviews 65, 701–717.

Wei, Q., Fan, H.R., Lan, T.G., Liu, X., Jiang, X.H., Wen, B.J., 2015. Genesis of Sizhuang gold deposit, Jiaodong Peninsula: evidences from fluid inclusion and quartz solubility modeling. Acta Petrologica Sinica 31, 1049–1062 (in Chinese with English abstract).

Xiao, W.J., Windley, B.F., Hao, J., Zhai, M.G., 2003. Accretion leading to collision and the Permian Solonker suture, Inner Mongolia, China: termination of the central Asian orogenic belt. Tectonics 22, 1069. http://dx.doi.org/10.1029/2002TC001484.

Yang, D.J., 2000. Characteristics and genesis of fine-clastic rock-type Au deposits in the Liaodong Rift. Acta Geologica Sinica 74, 570–575.

Yang, J.H., Zhou, X.H., Chen, L.H., 2000. Dating of gold mineralization for super-large altered tectonic-type gold deposits in Northwestern Jiaodong Peninsula and its implications for gold metallogeny. Acta Petrologica Sinica 16, 454–458 (in Chinese with English abstract).

Yang, L.Q., Deng, J., Zhang, J., Wang, Q.F., Gao, B.F., Zhou, Y.H., Guo, C.Y., Jiang, S.Q., 2007. Preliminary studies of fluid inclusions in Damoqnjia gold deposit along Zhaoping fault zone, Shandong province, China. Acta Petrologica Sinica 23, 153–160 (in Chinese with English abstract).

Yang, L.Q., Deng, J., Guo, C.Y., Zhang, J., Jiang, S.Q., Gao, B.F., Gong, Q.J., Wang, Q.F., 2009. Ore-forming fluid characteristics of the Dayingezhuang gold deposit, Jiaodong gold province, China. Resource Geology 59, 182–195.

Yang, L.Q., Deng, J., Wang, Z.L., Zhang, L., Guo, L.N., Song, M.C., Zheng, X.L., 2014a. Mesozoic gold metallogenic system of the Jiaodong gold province, eastern China. Acta Petrologica Sinica 30, 2447–2467 (in Chinese with English abstract).

Yang, L.Q., Deng, J., Wang, Z.L., 2014b. Ore-controlling structural pattern of Jiaodong gold deposits: geological-geophysical integration constraints. In: Chen, Y.T., Jin, Z.M., Shi, Y.L., Yang, W.C., Zhu, R.X. (Eds.), The Deep-Seated Structures of Earth in China. Sciences Press, Beijing, pp. 1006–1030 (in Chinese).

Yang, L.Q., Deng, J., Goldfarb, R.J., Zhang, J., Gao, B.F., Wang, Z.L., 2014c. $^{40}Ar/^{39}Ar$ geochronological constraints on the formation of the Dayingezhuang gold deposit: new implications for timing and duration of hydrothermal activity in the Jiaodong gold province, China. Gondwana Research 25, 1469–1483.

Yang, L.Q., Deng, J., Wang, Z.L., Guo, L.N., Li, R.H., Groves, D.I., Danyushevskiy, L., Zhang, C., Zheng, X.L., Zhao, H., 2016a. Relationships between gold and pyrite at the Xincheng gold deposit, Jiaodong Peninsula, China: implications for gold

source and deposition in a brittle epizonal environment. Economic Geology 111 (1), 105–126.
Yang, L.Q., Deng, J., Qiu, K.F., Ji, X.Z., Santosh, M., Song, K.R., Song, Y.H., Geng, J.Z., Zhang, C., Hua, B., 2015a. Magma mixing and crust-mantle interaction in the Triassic monzogranites of Bikou Terrane, central China: constraints from petrology, geochemistry, and zircon U-Pb-Hf isotopic systematics. Journal of Asian Earth Sciences 98, 320–341.
Yang, L.Q., Ji, X.Z., Santosh, M., Li, N., Zhang, Z.C., Yu, J.Y., 2015b. Detrital zircon U-Pb ages, Hf isotope, and geochemistry of Devonian chert from the Mianlue Suture: implications for tectonic evolution of the Qinling orogen. Journal of Asian Earth Sciences. http://dx.doi.org/10.1016/j.jseaes.2015.04.013.
Yang, L.Q., Deng, J., Wang, Z.L., Zhang, L., Goldfarb, R.J., Yuan, W.M., Weinberg, R.F., Zhang, R.Z., 2016b. Thermochronologic constraints on evolution of the Linglong Metamorphic Core Complex and implications for gold mineralization: a case study from the Xiadian gold deposit, Jiaodong Peninsula, eastern China. Ore Geology Reviews 72, 165–178. http://dx.doi.org/10.1016/j.oregeorev.2015.07.006.
Yardley, B.W.D., Cleverley, J.S., 2014. The Role of Metamorphic Fluids in the Formation of Ore Deposits. Special Publications, Geological Society, London. http://dx.doi.org/10.1144/SP393.5.
Zen, E.A., Hammarstrom, J.M., 1984. Magmatic epidote, its petrologic significance. Geology 12, 515–518.
Zhai, M.G., Santosh, M., 2011. The early Precambrian odyssey of the North China Craton: asynoptic overview. Gondwana Research 20, 6–25.
Zhang, L.G., 1985. The Application of the Stable Isotope to Geology: the Hydrothermal Mineralization of Metal Activation and it's Prospecting. Shaanxi Science and Technology Publishing House, Xi'an, pp. 1–267 (in Chinese).
Zhang, L.G., 1989. Petrogenetic and Minerogenetic Theories and Prospecting: Stable Isotopic Geochemistry of Main Type Ore Deposit and Granitoids of China. Press of Beijing University of Technology, Beijing, pp. 1–200 (in Chinese).
Zhang, T., Zhang, Y.Q., 2007. Geochronological sequence of Mesozoic intrusive magmatism in Jiaodong Peninsula, its tectonic constraints. Geological Journal of China Universities 13, 323–336 (in Chinese with English abstract).
Zhang, L.C., Sheng, Y.C., Li, H.M., Zeng, Q.D., Li, G.M., Liu, T.B., 2002. Helium andargon isotopic compositions of fluid inclusions and tracing to the source ofore-forming fluids for Jiaodong gold deposits. Acta Petrologica Sinica 18, 559–565 (in Chinese with English abstract).
Zhang, H.Y., Hou, Q.L., Cao, D.Y., 2007. Tectono-chronologic constraints on a Mesozoic slip, thrust belt in the eastern Jiaodong Peninsula. Science in China (Series D) 50, 25–32.
Zhang, L.C., Zhou, X.H., Ding, S.J., 2008. Mantle-derived fluids involved in large-scale gold mineralization, Jiaodong District, China: constraints provided by the He–Ar and H–O isotopic systems. International Geology Review 50, 472–482.
Zhang, J., Zhao, Z.F., Zheng, Y.F., Dai, M., 2010. Postcollisional magmatism: geochemical constraints on the petrogenesis of Mesozoic granitoids in the Sulu orogen, China. Lithos 119, 512–536.
Zhang, C., Liu, Y., Liu, X.D., Feng, J.Q., Huang, T., Zhang, Q., Wang, X.D., 2014. Characteristics of sulfur isotope geochemistry of the Xincheng gold deposit, Northwest Jiaodong, China. Acta Petrologica Sinica 30, 2495–2506 (in Chinese with English abstract).
Zhao, G.C., Wilde, S.A., Cawood, P.A., Sun, M., 2001. Archean blocks and their boundaries in the North China Craton: lithological, geochemical, structural and P–T path constraints and tectonic evolution. Precambrian Research 107, 45–73.
Zhao, G.C., Sun, M., Wilde, S.A., Li, S.Z., 2005. Late Archean to Paleoproterozoic evolution of the North China Craton: key issues revisited. Precambrian Research 136, 177–202.
Zhou, Z.J., Chen, Y.J., Jiang, S.Y., Zhao, H.X., Qin, Y., Hu, C.J., 2014. Geology, geochemistry and ore genesis of the Wenyu gold deposit, Xiaoqinling gold field, Qinling Orogen, southern margin of North China Craton. Ore Geology Reviews 59, 1–20.
Zhu, G., Niu, M.L., Xie, C.L., Wang, Y., 2010. Sinistral to normal faulting along the Tan-Lu Fault Zone: evidence for geodynamics witching of the East China continental margin. The Journal of Geology 118, 277–293.